catalysts

MDPI

Review

Catalytic Materials for Gasoline Particulate Filters Soot Oxidation

Roberto Matarrese

Laboratory of Catalysis and Catalytic Processes, Dipartimento di Energia, Politecnico di Milano, via La Masa 34, 20156 Milano, Italy; roberto.matarrese@polimi.it

Abstract: The energy efficiency of Gasoline Direct Injection (GDI) engines is leading to a continuous increase in GDI engine vehicle population. Consequently, their particulate matter (soot) emissions are also becoming a matter of concern. As required for diesel engines, to meet the limits set by regulations, catalyzed particulate filters are considered as an effective solution through which soot could be trapped and burnt out. However, in contrast to diesel application, the regeneration of gasoline particulate filters (GPF) is critical, as it occurs with almost an absence of NO_x and under oxygen deficiency. Therefore, in the recent years it was of scientific interest to develop efficient soot oxidation catalysts that fit such particular gasoline operating conditions. Among them ceria- and perovskite-based formulations are emerging as the most promising materials. This overview summarizes the very recent academic contributions focusing on soot oxidation materials for GDI, in order to point out the most promising directions in this research area.

Keywords: soot oxidation; gasoline; GDI; GPF; ceria-based catalysts; perovskite-type catalysts; emissions reduction; environmental catalysis

Citation: Matarrese, R. Catalytic Materials for Gasoline Particulate Filters Soot Oxidation. *Catalysts* **2021**, *11*, 890. https://doi.org/10.3390/catal11080890

Academic Editor: Valeria Di Sarli

Received: 22 June 2021
Accepted: 19 July 2021
Published: 22 July 2021

1. Introduction

In recent years, Gasoline Direct Injection (GDI) engines have gained popularity in relation to their high fuel economy, reduced CO_2 emissions, and improved performance when compared to traditional gasoline Port Fuel Injection (PFI) and Multi Point Injection (MPI) engines. In particular, the GDI market of light-duty vehicles is continuously increasing worldwide, forced by the greenhouse gas emission reduction policies as it is shown in Figure 1.

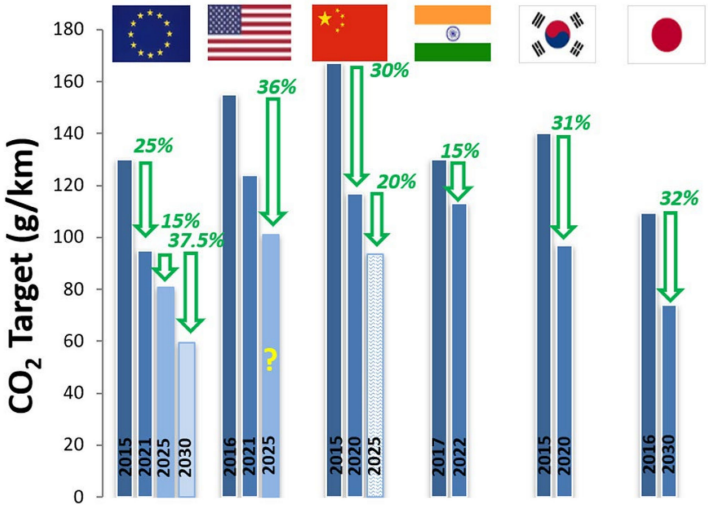

Figure 1. Summary of CO_2 targets for light-duty passenger cars in major markets. Reproduced with permission of reference [1].

As a result, in 2017, for the first time, GDI passenger cars exceeded sales of diesel cars (51% vs. 44%) in the EU, while in the decade between 2008 and 2018 the market share of GDI vehicles increased from 2.3% to 51% in the US where, according to the EPA estimates, more than 90% of vehicles will be equipped with GDI engines by 2025 [2–5].

However, despite the benefits of reduced fuel consumption and CO_2 emissions, GDI engines have also some drawbacks. The most concern is related to the higher amount of soot formation than port fuel injection engines, which is mainly due to the existence of fuel-rich regions in the combustion chamber, and to liquid fuel impingement onto the piston and cylinder surfaces, leading to incomplete combustion [2,3,6,7]. In particular, the particulate number (PN) emissions (i.e., especially the smaller particles) of GDI engines can exceed more than ten times that of conventional gasoline engines, as well as that of diesel engines fitted with diesel particulate filters (DPFs) (see Figure 2) [8].

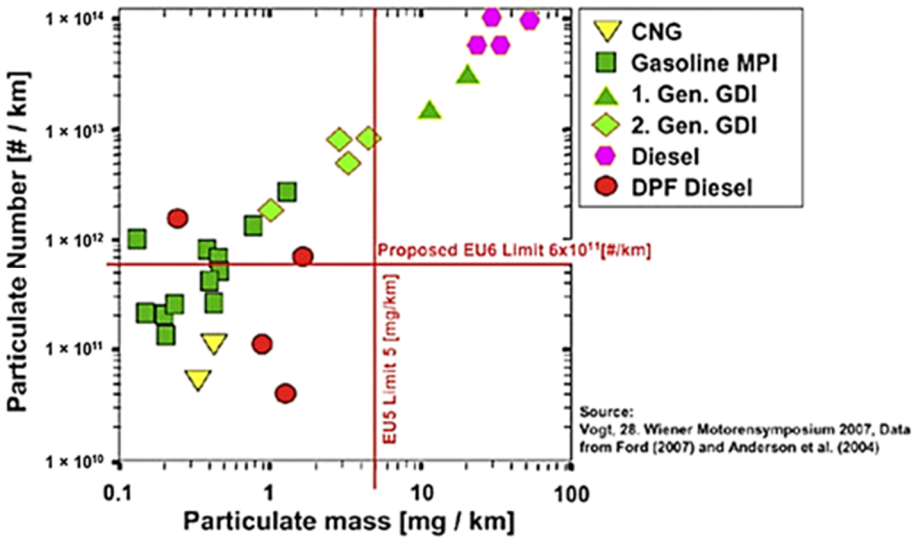

Figure 2. Comparison of particulate number and particulate mass emissions for gasoline and diesel engines. Adapted and reproduced with permission of reference [9].

Owing to GDI vehicles spreading, and in relation to the well-known environmental problems and human health effects of particulates, GDI were included in particulate matter legislation in most of the advanced automotive markets. Europe extended limitations for particle mass (PM) emissions to GDI, starting with the Euro 5 standards (i.e., 5 mg/km and 4.5 mg/km according to Euro 5a and Euro 5b from September 2009 and September 2011, respectively). Euro 6b standards also set limits for PN emissions (i.e., 6×10^{12} #/km from September 2014). Then, more stringent limits were imposed in September 2017 with Euro 6c standards, which reduced PN emissions down to 6×10^{11} #/km. Along the same lines, the US and China also proposed more stringent emission regulations for GDI vehicles (e.g., CARB, level III, and China 6 standards, respectively) [3,7,9,10].

For these reasons, considerable efforts have been devoted in recent years to limit particulate matter emissions from GDI engines through the improvement of the technological level of the engines [7] or by means of suitable after-treatment technologies [2,9] (see Figure 3).

With respect to engine modifications, the optimization of air-fuel mixing via improved fuel injection strategy (e.g., multiple injections, injection time, and pressure) was indicated as a key factor to limit particulate emissions, particularly when the engine is cold or warming up [8,11]. In this optical, dual injection systems which combine GDI and PFI have been proposed for their superior combustion performance and potential to decrease particulate matter formation [12]. In parallel to the developments in vehicular technologies, the possibility to change fuel properties and composition (e.g., oxygen content, aromatic content, and volatility) was also considered to decrease particulate matter emission. On the

one hand, there is a general consensus that particulate matter formation increases upon increasing aromatics content. On the other hand, despite several studies indicating the reduction in particulate matter emission by using ethanol-gasoline blended fuels, the debate is still open due to the complex interactions existing between fuel properties and vehicles characteristics [5,10,13].

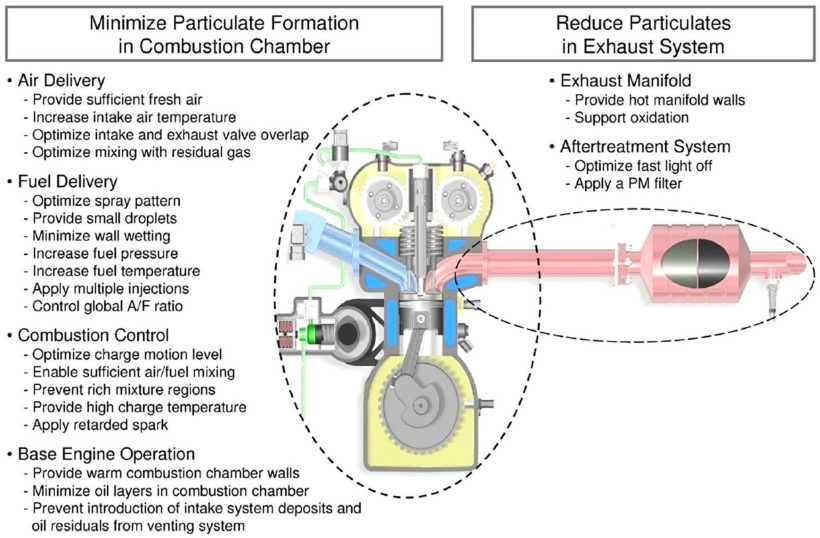

Figure 3. Strategies to minimize particulate emission from gasoline engines. Reproduced with permission of reference [7].

Despite the development of new engines, equipped with more efficient injection systems and with novel combustion technologies, can impact the reduction in particulate matter emissions, gasoline particulate filters (GPFs) placed in the after-treatment system are currently considered as the most effective solution to comply with the strict emissions standards.

GPFs are devices similar to the well-established diesel particulate filters (DPFs) [14]: honeycomb-like ceramic structures, usually made of cordierite, with the channels blocked at alternate ends which physically capture the particulate and need to be periodically regenerated to avoid pressure drops. However, despite the similar working principle, GPFs differ from DPFs due to several differences between gasoline and diesel exhausts [2,5,9,15]. Gasoline engines have lower particulate emissions than diesel engines (i.e., both particulate mass and particulate numbers) resulting in a thinner soot layer formation which, on one side, can lead to longer GPF conditioning time and thus lower the filtration efficiency but, on the other hand, provides lower pressure drops.

In addition, there are also substantial differences between GPFs and DPFs in terms of the regeneration process.

In diesel applications, the regeneration can be achieved by increasing the filter temperature (active regeneration) so that the particulate is burnt by the oxygen present in the exhaust gases (Reactions (1) and (2)):

$$C + O_2 \rightarrow CO_2 \quad (1)$$

$$C + \frac{1}{2} O_2 \rightarrow CO \quad (2)$$

However, this process requires an extra fuel consumption, resulting in reduced fuel efficiency. Alternatively, the use of catalytic filters, in which DPFs are coated with a catalytic layer that favors the particulate oxidation at lower temperatures (passive regeneration), has been proposed in order to limit filter overheating and fuel consumption during the regeneration phase. In particular, aiming at the low-temperature oxidation of soot, the ex-

ploitation of NO_2 as soot oxidizing agent has been considered, NO_2 being a stronger oxidant than oxygen [16] (Reactions (3) and (4)):

$$C + 2NO_2 \rightarrow 2NO + CO_2 \quad (3)$$

$$C + NO_2 \rightarrow NO + CO \quad (4)$$

To this end, catalytic DPFs are often coated with Pt-based catalysts [17] which promote (i) the oxidation of NO (i.e., either in the exhaust gases, or formed in Reactions (3) and (4)) to NO_2 (Reaction (5)), as well as (ii) the oxidation of CO formed in Reactions (2) or (4) to CO_2.

$$NO + 1/2O_2 \rightarrow NO_2 \quad (5)$$

As regards gasoline applications, exhaust temperatures are relatively higher than those of their diesel counterparts (i.e., up to 900 °C compared to < 400 °C for diesel [2]). These temperatures are high enough to sustain passive regeneration, i.e., without the use of an outside energy source typical of the active regeneration for diesel. However, unlike diesel engines, where oxygen is in excess and exhaust contain high amounts of NO_x, gasoline engines, in most cases, run close to stoichiometry conditions and contain negligible NO_x (due to the presence of the up-stream three-way catalysts (TWC)). Consequently, the lower O_2 concentration makes GDI regeneration more critical under high load, and effective mainly during vehicle deceleration, where the fuel is cut-off and oxygen becomes available in the exhaust.

For these reasons, DPF technology could not be directly used as it was for GDI engines, and preliminary adjustments to the filter parameters, i.e., GPF materials, design, and configuration, were due to be taken into account [2].

GPFs were first commercialized by Daimler on their Mercedes-Benz S500 luxury sedan in 2014 [18]; currently they are rapidly spreading in the GDI after-treatment systems, particularly in Europe and China [1,19,20]. Initially, research and applications focused on bare GPFs that were retrofit behind a TWC, in the close-coupled or in the underfloor position (Figure 4) [2,21]. GPFs to address particulate emissions from lean-burn GDI engines have been also investigated [1,21]. Subsequently, catalyzed filters (i.e., DPFs coated mostly with a TWC layer) were also considered (Figure 4) aimed, on one hand, at improving both the particulate regeneration and filtration efficiencies (i.e., by lowering the soot oxidation temperature and exploiting the catalyst as a filtration layer, respectively) and, on the other hand, at improving the reduction of gaseous emissions [22–26].

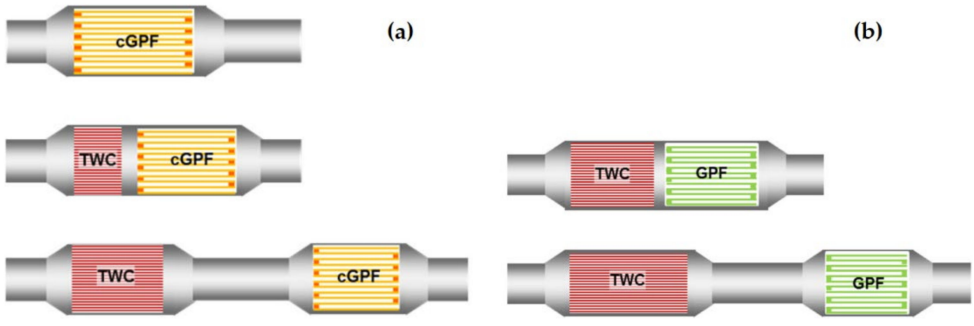

Figure 4. Gasoline system architecture with GPF: TWC-coated cGPF (**a**) and uncoated GPF systems (**b**). From reference [21].

The development of integrated catalytic systems with both GPF and TWC functions combined in a single catalyst brick (e.g., sometimes denoted as four-way catalysts), instead of the series converter configuration, has been also proposed. One example of four-way converter was launched by Volkswagen, who introduced catalyzed GPF in its up! GTI city car in the 2018 [27].

Despite catalyzed GPFs are beginning to be used at a commercial scale, investigations on catalytic materials for GDI applications are still scarce, and mostly limited to technical papers dealing with TWC coated filters. Moreover, in spite of the fact that many fundamental studies are available in the literature concerning catalytic materials for diesel soot oxidation (e.g., see the reviews [28–31]), minor academic studies were focused on gasoline soot applications. Only in the last five years, given the renewed interest in GDI technology, an increasing number of studies have been published focusing on catalytic materials suited for soot oxidation under gasoline exhaust conditions. As for diesel applications, low temperature activity and high CO_2 selectivity on one hand, and high thermal stability on the other, represent the main key issues for the development of suitable catalytic materials for soot oxidation. In addition, the specific scientific issue for gasoline applications consists in the development of catalysts effective for soot oxidation with low partial pressure of oxygen, or even in the total absence of oxygen, and nearly no NO_x. According to the literature, these special GDI working conditions (i.e., oxygen/NO_2-lacking conditions) disfavor the application of the well-developed Pt-based soot oxidation diesel catalysts which rely on NO_2–O_2–soot reactions, and has driven the development of alternative soot-oxidation catalysts. For this reason, among the different noble metal-free catalysts proposed for soot oxidation (e.g., see the reviews [28–31]), ceria-based oxide formulations and mixed oxides with perovskite structure were specifically selected as most promising materials for GPFs, on the basis of their outstanding oxygen storage/red-ox properties that allow efficient oxygen delivery onto the soot surface, even under the severe GDI exhaust requirements.

With these premises, this review focuses on soot oxidation catalysts for GDI, and discusses their property–activity relationships in order to summarize the recent developments and promising directions in this research area.

2. Ceria-Based Catalysts for Gasoline Soot Oxidation

Ceria-based oxides are among the most extensively investigated catalysts for the O_2-assisted soot oxidation in DPF applications (e.g., see the reviews [31–33]). The success of ceria-based materials for soot oxidation is strictly correlated to the ceria oxygen storage properties and to its ability to change oxidation state (i.e., by the Ce^{4+}/Ce^{3+} redox cycle). In particular, the generation of active oxygen species (O_x^-) upon activation of gas phase oxygen over surface oxygen vacancies of reduced ceria has been indicated as a key step for soot oxidation. In addition, doping ceria with proper foreign cations (i.e., Zr or other rare earth elements (e.g., Y, La, Pr, and Nd)) it is widely accepted to positively affect its catalytic behavior by improving oxygen storage/redox properties and also thermal stability. Although ceria-based materials have been thoroughly studied for diesel soot oxidation, their application for GPFs (i.e., under low oxygen availability) has only been specifically investigated in the last few years.

Wang et al. [34] were among the first to study CeO_2-based materials for soot combustion under gasoline engine conditions. In particular, they investigated a series of $wCeO_2$-(1–w)ZrO_2 (w = 0–100% mass fraction) catalysts by temperature-programmed oxidation (TPO) experiments with low O_2 content (i.e., reduced until 1% v/v) under loose contact conditions. Among all the investigated catalysts, the 70%CeO_2-30%ZrO_2 sample showed the best catalytic activity for soot combustion with T_i (i.e., ignition temperature), T_m (the temperature corresponding to the maximum in the TPO profile), and T_f (the temperature corresponding to the complete oxidation) at 486, 625, and 722 °C, respectively, vs. 602, 719, and 795 °C, for un-catalyzed soot combustion. According to oxygen storage (OCS) and H_2-TPR experiments, this result was correlated with both the high OCS capacity and the good reducibility of 70%CeO_2-30%ZrO_2. In addition, XPS analysis showed that 70%CeO_2-30%ZrO_2 had the largest amount of both surface Ce^{3+}, which was related to the creation of oxygen vacancies, and surface-adsorbed oxygen, that were indicated to be beneficial for soot oxidation under low oxygen concentration condition. This material also showed a good thermal stability, as only minimal degradation of the soot combustion activity was found upon increasing the calcination temperature in the 600–900 °C range.

Sun Park et al. [35] confirmed the positive effect of Zr doping on Ceria. They investigated macroporous Ce–Zr mixed oxides with Zr contents in the 0, 30%, 50%, 70%, and 100% molar range, and evaluated their catalytic activities for soot oxidation by TPO with 1% O_2 under tight conditions in the presence and absence of water. Under dry conditions, catalysts with 30% and 50% of Zr showed the best performance: T_{50} and T_m were observed near 425–435 °C, compared to 590–610 °C for non-catalyzed soot, and 445–455 °C for bare ceria. A clear relationship between soot oxidation activity and both the large amounts of surface-active oxygen (O_x^-) and oxygen vacancies was pointed out according to O_2-TPD, H_2-TPR and XPS analyses. Under wet conditions (1% O_2, 10% H_2O), the performance of all the catalysts improved. In particular, the activity of ceria showed the greatest increase, showing similar activity to catalysts with 30% and 50% of Zr (i.e., T_{50} and T_m were observed near 410 and 420 °C, respectively). XPS analyses were also performed on samples aged under wet conditions, and revealed an increase in both surface active oxygen and oxygen vacancies after wet conditions pretreatment. According to isotopic experiment with $H_2{}^{18}O$ and DTF calculations, this increase was ascribed to H_2O adsorption, followed by H_2O dissociation resulting in the formation of additional active oxygen, beneficial for soot oxidation. Finally, the effect of thermal aging at 800 °C was investigated for pure ceria and for the sample containing 30% of Zr. Both thermally treated catalysts showed decreased catalytic activity under dry conditions. According to the XPS results, this was ascribed to the reduction in both the amounts of surface-active oxygen and oxygen vacancies which, in turn, were related to the catalyst sintering at high temperatures, as it was revealed by XRD and N_2-adsorption/desorption analyses. Additionally, in the presence of water, both the aged catalysts showed higher activity than those observed under dry conditions. In particular, the performance of the thermal treated Zr-containing system was the same as that of a fresh catalyst, while thermal treated ceria showed a lower activity than fresh ceria. These results, on the one hand, confirmed the direct participation of water in soot oxidation, regardless of the pre-existing oxygen vacancies, and, on the other hand, revealed that the mechanism of soot oxidation in the presence of H_2O is deeply related to the contact points between the soot and catalysts. Accordingly, from HR-SEM analyses, the macroporous structure of ceria was found to partially collapse after aging, thus leading to deactivation as a result of the loss of contact points. On the contrary, the Zr-containing sample exhibited high thermal stability, still maintaining its macroporous structure after aging which is essential for preserving the soot–catalyst contact and thus the soot oxidation activity.

The effect of Zr substitution on soot combustion over nanostructured ceria was also investigated by Liu et al. [36]. For this purpose, the activity of $Ce_{0.92}Zr_{0.08}O_2$ and $Ce_{0.84}Zr_{0.16}O_2$ samples was compared with that of pure CeO_2 under tight conditions. Both soot-TPO (i.e., with 10% O_2) and soot-TPR (i.e., with only N_2) experiments showed the reactivity order $Ce_{0.92}Zr_{0.08}O_2$ > $Ce_{0.84}Zr_{0.16}O_2$ > CeO_2. In particular $Ce_{0.92}Zr_{0.08}O_2$ showed the best catalytic activity, with T_m at 355 °C and T_i at 290 °C during TPO and TPR experiments, respectively. In other words, Zr substitution was confirmed to improve the catalytic activity, but excess Zr showed an inhibition effect. First of all, according to SEM and TEM analyses, the beneficial role of Zr was related to the formation of smaller agglomerates for $Ce_{1-x}Zr_xO_2$ samples (i.e., average size of ca. 60 nm vs. ca. 165 nm for pure CeO_2) which are expected to provide a larger external surface and increased intraparticle voids, and consequently higher soot–ceria contact, thus improving soot combustion activity. In addition, XPS, Raman, and O_2-TPD analyses showed that Zr substitution favors the formation of surface oxygen vacancies, the migration of lattice oxygen (O^{2-}) and, thus, the generation of more active oxygen species (O_2^- and O^-) for soot oxidation over both $Ce_{1-x}Zr_xO_2$ samples. However, based on H_2-TPR profiles, excess Zr was found to penalize surface reducibility. As a matter of fact, higher reduction temperature and lower H_2 consumption for surface Ce^{4+} reduction were found for $Ce_{0.84}Zr_{0.16}O_2$ (i.e., 371 °C, 0.44 mmol H_2/g) than $Ce_{0.92}Zr_{0.08}O_2$ (342 °C, 0.62 mmol H_2/g). Accordingly, extra Zr, with strong electronegativity (i.e., higher than Ce), was suggested to inhibit the mobility of lattice oxygen from the bulk to the surface resulting in the decrease in soot oxidation activity.

Liu et al. [37] worked on CeO_2 and Ce/Zr mixed oxides, focusing on the specific role of surface oxygen vacancies on catalytic soot oxidation. Both TPO and isothermal experiments with 1% O_2 showed the higher reactivity and stability of pure CeO_2 in comparison to the Zr-doped systems, under tight conditions. In particular, in the soot-TPO tests, the T_m was found to be near 430 °C for CeO_2 and above 460 °C for Ce/Zr catalysts. The detrimental effect of Zr doping was correlated with the excessive formation of surface oxygen vacancies which was based on both XPS and H_2-TPR analyses. On the one hand, Ce 3d XPS results showed higher amounts of Ce^{3+} for the Zr-containing samples, which was closely related to the formation of surface oxygen vacancies. This was further confirmed by the O 1s XPS results, which showed higher quantities of O^{2-} in oxygen vacancies for the Ce/Zr samples. On the other hand, the H_2-TPR results pointed out that the introduction of Zr resulted in the formation of higher amounts of O^{2-} surface species rather than highly active O_x^- species which was likely related to high content of surface oxygen vacancies. Consequently, the authors suggested the medium surface vacancies concentration for ceria-based catalysts as a good prerequisite for GPF applications.

Aneggi et al. [38] carried out studies on $Ce_{0.8}Zr_{0.2}O_2$ and ZrO_2 focusing on the effect of oxygen concentration (i.e., 0% O_2/N_2, 1% O_2/N_2, and air) and of the type of soot/catalyst contact. For this purpose, three different contact conditions were employed with different degrees of carbon/catalyst interactions: in addition to the well-known loose contact (i.e., obtained by mixing soot and catalyst in a vial) and tight contact (i.e., obtained by grinding the mixture in an agate mortar) conditions, a third type of mixing was also realized by milling soot–catalyst powders in a high-energy mill (i.e., supertight contact conditions). Both thermal gravimetric analyses (TGA) and TPO results showed that ceria–zirconia overtakes bare ZrO_2 in both soot oxidation activity and CO_2 selectivity, and that it is less influenced by the variation of the oxygen concentration. In particular, under inert conditions (i.e., 0% O_2/N_2), soot combustion was negligible for zirconia/soot mixtures, regardless of the contact type. Conversely, significant activity was observed for ceria–zirconia/soot mixtures, with T_{50} (i.e., the temperature required to reach 50% soot conversion) of 775, 546, and 420 °C under loose, tight, and supertight contact conditions, respectively. The introduction of oxygen promoted oxidation for all formulations, particularly for zirconia, and in a minor extent for ceria–zirconia. As a matter of fact, in the case of zirconia, the T_{50} decreased by ca. 80 °C in air (i.e., vs. 1% O_2/N_2), while for ceria–zirconia only a slight decrease of ca. 30 °C was observed. According to OCS and H_2-TPR analyses, the higher soot oxidation activity of ceria–zirconia (i.e., a highly reducible material) was attributed to the higher availability of both lattice and surface oxygen in comparison of pure zirconia (i.e., a non-reducible material). Thus, unlike zirconia, ceria–zirconia-based systems were suggested to use the surface/bulk oxygen to oxidize soot, even in the absence of oxygen in the gas phase, through the oxidation of carbon at the catalyst interface with the formation of an oxygen vacancy. Then, under oxygen rich conditions the resulting vacancies can be the centers for the activation of gas phase oxygen with the formation of active oxygen species that promote soot oxidation. Another interesting feature was pointed out by H_2-TPR experiments performed over ceria–zirconia–soot mixtures, which revealed that the reduction peak for bare ceria–zirconia centered at ca. 560 °C progressively shifts down to ca. 530, 505, and 420 °C for loose, tight, and supertight contact conditions, respectively. These results suggest that, under low oxygen contents, the presence of soot can act as a reducing center by favoring the reduction in the catalyst and the formation of oxygen vacancies, thus increasing the overall surface/bulk oxygen utilization and consequently soot combustion, i.e., even under conditions typical of GDI engine exhaust.

Ceria–praseodymia mixed oxides were also proposed for GPF applications. Martínez-Munuera et al. [39] investigated two series of $Ce_{1-x}Pr_xO_2$ catalysts (x = 0.2, 0.3, 0.4, 0.5, 0.6, 0.7, 0.8, 0.9, and 1) prepared by using two methods of synthesis, i.e., classic co-precipitation method and direct calcination of precursors. The soot combustion activity was monitored by TPD in He, both under loose and tight contact conditions. The TPD results were analyzed in detail by considering analogous TPD experiments performed in the absence of

soot, which allowed to quantify the O_2 emissions under inert atmosphere and to establish their role in soot combustion. According to O_2-TPD results, the addition of praseodymium to the ceria was found to enhance the oxygen catalysts' mobility, favoring the O_2 release under inert atmosphere. In particular, the overall O_2 release was found to increase upon increasing the Pr content, particularly at low Pr contents, and regardless of the methods of preparation. With regard to soot combustion activity, all catalysts were able to oxidize soot under inert atmosphere at low temperatures, even under loose contact conditions. As a matter of fact, soot ignition temperatures near 300 °C were observed, i.e., ca. 150 °C lower than that obtained for the un-catalyzed soot oxidation in the presence of gas-phase oxygen. This was ascribed to the direct role of oxygen released from the catalysts into soot combustion. Soot oxidation was further promoted at high temperatures, as a shift of the combustion curves (i.e., CO_2 evolutions) towards lower temperatures was observed if compared with the O_2 emissions profiles collected during O_2-TPD. Soot combustion was greatly enhanced under tight conditions so that soot ignition temperatures were further shifted near 200 °C, i.e., ca. 100 °C lower than under loose contact conditions. Moreover, in this case, more O_2 than that evolving from O_2-TPD under inert atmosphere was involved in the soot combustion process. Accordingly, the results obtained under the more severe conditions (higher temperatures or tight contact conditions) highlighted the role of soot acting as a "driving force" in promoting lattice oxygen delivery/transfer from these catalysts and, as a result, soot combustion. Ultimately, from the bulk of the results, ceria–praseodymia mixed oxides emerged as promising catalysts under the demanding GDI exhaust conditions (i.e., under limited oxygen contents).

The effect of Pr doping in CeO_2 was also studied by Sartoretti et al. [40]. In this case, a nanostructured equimolar ceria–praseodymia catalyst was prepared via hydrothermal synthesis. Soot oxidation results obtained both with TPO and isothermal oxidation tests under low O_2 concentration (i.e., 1%) confirmed the beneficial effect of Pr, which allowed a remarkable activity increase with T_{50} of 510 °C in loose contact conditions (vs. ca. 650 °C for bare soot) and 465 °C in tight contact conditions (vs. 485 °C for pure CeO_2). Additionally, CO_2-selectivity was increased above 95% (vs. almost complete CO selectivity for un-catalyzed soot oxidation). According to H_2- and CO-TPR results, this enhanced activity was attributed to the increase of ceria reducibility resulting from doping with Pr. In particular, the H_2 reduction profile of Pr-doped ceria showed a single peak centered at ca. 460 °C, contrary from pure ceria, which typically presents two peaks, one at around 500 °C, which is attributed to surface reduction, and another above 700 °C, which is assigned to bulk reduction. Thus, Pr addition was suggested to weaken the Ce–O bond, thus fostering the oxygen release and consequently its availability during the soot oxidation reaction.

The incorporation of Mn into ceria/zirconia systems was also evaluated. Yao et al. [41] studied CeO_2–ZrO_2–MnO_x mixed oxides with different MnO_x content (0, 10, 15, and 100 wt%), synthesized by co-precipitation method. The structural and redox properties of the mixed oxides were investigated by means of XRD, BET, H_2-TPR, O_2-storage capacity, O_2-TPD, Raman, and XPS measurements. In addition, TPO tests were performed under low O_2 concentration (i.e., 0.5%) to evaluate the catalytic activity for soot oxidation. Mixed CeO_2–ZrO_2–MnO_x catalysts showed better soot conversion compared with pure MnO_x and CZ catalysts. In particular, the best performance was obtained with 10% MnO_x doping, which led to T_{50} near 340 °C and 520 °C under tight and loose contact conditions, respectively. The poor reactivity of bare MnO_x was correlated with its low BET surface, which is likely responsible for the weak contact efficiency between catalyst and soot. Additionally, the superior activity of the MnO_x-modified catalysts compared to bare CeO_2–ZrO_2, was mainly attributed to the capability of generation and movement of reactive oxygen species which are crucial for soot oxidation, particularly under a low oxygen concentration environment. At first, this improvement was related to the change in the redox properties of CeO_2, as the addition of MnO_x was found to decrease the onset temperature of the reduction in H_2. Moreover, MnO_x doping favored both oxygen storage capacity and oxygen desorption capacity at low

temperatures, which was consistent with the high amount of oxygen vacancies and surface oxygen species, as revealed by Raman and XPS analyses.

Of note, the specific soot oxidation activity of pure Mn-based catalysts was investigated by Yang et al. [42], who compared α-Mn_2O_3 samples synthesized using different methods, i.e., selective dissolution method (SD) and traditional sol–gel (SG) or direct calcination (DC) methods. TPO results with 1% O_2 showed the reactivity trend SD > SG > DC under loose contact conditions. In fact, SD–Mn_2O_3 exhibited the lowest T_{50} (630 °C vs. 640 °C and 661 °C) and also the best CO_2 selectivity (99.7% vs. 68.1% and 64.6%) compared with the other two samples. According to O_2-TPD analyses, the higher amounts of surface lattice oxygen and oxygen adsorbed on vacancies for SD–Mn_2O_3 were indicated as responsible for better redox properties and soot activity, as well. This was confirmed by H_2-TPR profiles for SD–Mn_2O_3 which were shifted to lower reduction temperatures if compared to SG–Mn_2O_3 and DC–Mn_2O_3. In addition, SEM analyses evidenced a sponge-like morphology with disorder-interconnected mesopores for the SD-catalyst which was indicated to favor CO diffusion and adsorption leading to increased CO oxidation by active surface oxygen and therefore to increased selective soot conversion to CO_2.

Additionally, the simultaneous doping of ceria/zirconia with La and Y was evaluated by Xiong et al. [43] who investigated CeO_2(45%)-ZrO_2(45%)-Y_2O_3(5%)-La_2O_3(5%) quaternary catalysts aged at different temperature from 600 to 1000 °C (i.e named CZ-600, CZ-700, CZ-800, CZ-900, and CZ-1000, respectively). The soot oxidation activity was investigated by TPO experiments with 1% O_2 focusing on the effect of structural properties, oxygen vacancies, O_2 adsorption/desorption ability, textural properties, and redox properties on the catalytic behavior. For further comparison, 10 wt% MnO_2/CZ-600 and MnO_2/CZ-800 catalysts (i.e., named Mn/CZ-600 and Mn/CZ-800, respectively) were prepared. The catalytic activity for soot conversion was found firstly to remain stable and then to decrease, upon increasing the aging temperature (i.e., CZ-600 ≈ CZ-700 ≈ CZ-800 > CZ-900 > CZ-1000). After the MnO_2 addition, Mn/CZ-600 and Mn/CZ-800 showed similar activity (T_{50} of ca. 360 °C under tight conditions), much better than that of CZ-600 and CZ-800 (T_{50} of ca. 390 °C), respectively. According to XPS and Raman analyses, there was no significant correlation between catalytic performance and the amount of surface oxygen vacancies. In addition, according to O_2-TPD experiments, neither the O_2 adsorption/desorption ability of these catalysts was found to directly affect their catalytic activity. On the contrary, the external surface area and the low-temperature reducibility (<500 °C) were the two major factors to influence the soot oxidation activity. In particular, the low activity observed for sample calcined at 900 °C and 1000 °C was correlated to their low external surface area, which was also suggested to decrease the catalyst–soot contact efficiency and soot oxidation capability. Furthermore, the existence of a critical value for the external surface area was indicated as essential for a proper soot oxidation activity. As a matter of fact, similar activity was observed from CZ-600 to CZ-800, despite CZ-600 showing higher external surface area than CZ-700 and CZ-800. In the same vein, Mn/CZ-600 showed a higher external surface area value than Mn/CZ-800, but similar activity. Therefore, the authors concluded that there might be a critical external surface value (i.e., between that of Mn/CZ-800 and CZ-900) that is likely to well disperse the soot particle. Anything higher than this critical value may not have a positive impact on the contact efficiency between catalysts and soot particles, while lower than this value would decline the contact efficiency and thus the catalytic activity of CZ-based catalysts. According to H_2-TPR results the drastic decline in soot oxidation activity for CZ-900 and CZ-1000 was also correlated to their lower low-temperature reducibility. Additionally, the superior catalytic performance of MnO_2-loaded catalysts was mainly ascribed to their much higher low-temperature reducibility. MnO_2-loaded CZ-based were definitively indicated as good catalysts applied to GPF, thanks to the synergistic effect of both external surface area and low-temperature reducibility on their catalytic performance.

Metal-Loaded Ceria-Based Catalysts

Different compounds (e.g., Ag, Co, and Cu) supported on ceria have been investigated as catalysts for diesel soot oxidation [30,32] and, recently, several studies have been related to their application under conditions typical of gasoline engines.

Liu et al. [44] investigated Ag(5 wt.%)/CeO_2 catalysts. In particular, two forms of morphology-controlled CeO_2 (i.e., nanocubes (NC) and spindles (sp)) were considered, which were compared with irregular-shaped CeO_2 nanoparticles (NP). Undoped catalysts were also investigated, for comparison purposes. Catalytic activity for soot oxidation was analyzed under isothermal conditions at 300 and 350 °C, followed by TPO with 1% O_2 in N_2 under tight contact conditions. The soot oxidation activity without Ag followed the order Ce–NP > Ce–NC > Ce–Sp at 300 °C; Ce–NP ≈ Ce–NC > Ce–Sp at 350 °C and Ce–NC > Ce–NP > Ce–Sp during the TPO. An excellent doping effect of Ag was reported. As a matter of fact, a 10-fold increase in the soot oxidation rate under isothermal conditions was reported for all the samples. The catalytic activity during TPO was found to follow the trend AgCe–NC > AgCe–NP > AgCe–Sp, as for undoped systems. This was also confirmed during TPO runs performed under more realistic conditions (i.e., loose contact mode). In particular the AgCe–NC catalyst showed the best activity with T_{50} of 450 °C. Notably partial deactivation was observed during isothermal experiments, which was more severe for doped and undoped NP- and Sp-based systems. The authors explained the different behavior (i.e., both activity and stability) of the investigated systems on the basis of the Mars–van Krevelen-like soot oxidation mechanism proposed for the ceria-based systems, in which (i) gas phase O_2 first adsorbs over ceria, then (ii) transforms into O_x^- species (either O^- or O_2^-), and finally (iii) spills, together with those coming from ceria lattice, onto soot to complete the oxidation process. Based on this mechanism, and according to H_2-TPR and Raman analyses, they correlated the higher activity and stability of Ce–NC system, compared to Ce–NP and Ce–Sp, to its more efficient generation of highly active O_2^- species. In addition, according to XPS analyses, the stronger tendency to deactivation observed for Ce–NP and Ce–Sp systems was related to their higher surface oxygen vacancies concentration. In fact, excessive ceria surface oxygen vacancies were suggested to inhibit the generation of O_2^- species with the preferential formation of less reactive O^- and O^{2-} species. Additionally, the catalyst–soot contact was indicated as essential for O_x^- transfer and thus responsible for the initial soot oxidation activity. On this basis, the authors explained the low performance of Ce–Sp in relation to its microporous structure resulting in the low accessibility of catalyst surface by soot. Accordingly, TEM analyses showed soot segregation on the catalyst surface. On the contrary, the higher oxidation capacity observed for Ce–NP and Ce–NC was correlated to their ability to homogenously mix with soot. Finally, the beneficial role of Ag doping was associated with the promotion of O_x^- and O_2^- species. In particular the AgCe–NC system was indicated as a promising catalyst for GDI applications, due to both its good activity and stability resulting from high O_x^- formation and their transformation into reactive O_2^-.

Aiming at elucidating the roles of both surface oxygen vacancies and active oxygen species (i.e., O_x^-) in soot oxidation, Wang et al. [45] investigated different Ag/CeO_2 catalysts with uniform structures but diverse surface oxygen vacancies contents, which were synthesized via a modified soot-containing solution combustion method. Depending on the soot amount added during the solution combustion process, the catalysts were denoted as AgCe-0, AgCe-0.01, AgCe-0.02, AgCe-0.03, AgCe-0.04, and AgCe-0.05, respectively. To explore the activity of the Ag/CeO_2 catalysts, soot-TPO tests under loose contact conditions with 1% O_2 were performed which showed the following activity order: AgCe-0.03 > AgCe-0.02 > AgCe-0.01 ≈ AgCe-0.04 > AgCe-0.05 > AgCe-0. In other words, the activity of Ag/CeO_2 catalysts was found to increase upon increasing the soot loaded during preparation showing a maximum with AgCe-0.03 (i.e., with T_m near 450 °C), and then decreasing as the soot amount increased further. This result was explained on the basis of XPS, Raman end H_2-TPR analyses. On the one hand, XPS revealed that the content of Ce^{3+} and, as a result, the amount of surface oxygen vacancies follows the or-

der AgCe-0.05 > AgCe-0.04 > AgCe-0.03 > AgCe-0.02 > AgCe-0.01 > AgCe-0. On the other hand, Raman and H_2-TPR results showed that AgCe-0.04 and AgCe-0.05 samples limited the generation of O_2^- species, compared with AgCe-0.03 followed by AgCe-0.02 and AgCe-0.01. This confirmed that although the presence of oxygen vacancies on the ceria surface is crucial for the generation of active O_x^- species, excessive oxygen vacancies induce the formation of less active O^- and ceria lattice oxygen O^{2-} rather than the highly reactive O_2^-. Consequently, AgCe-0.03, with moderate surface oxygen vacancies, exhibited the best activity (see Figure 5).

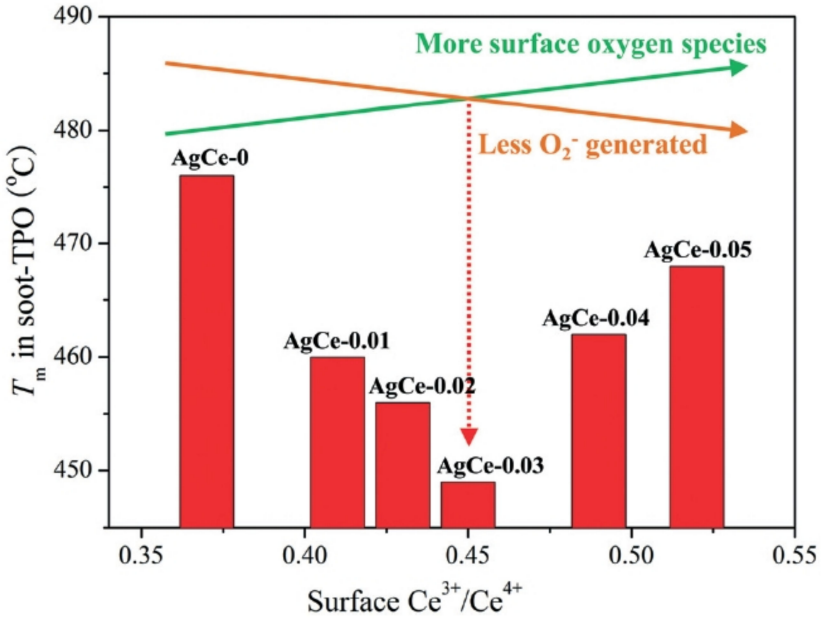

Figure 5. Schematic explanation for soot oxidation over Ag/CeO_2 catalysts with different contents of surface Ce^{3+}. Reproduced with permission of reference [45].

Isothermal soot oxidation experiments were also performed at 300 °C. AgCe-0, AgCe-0.01, AgCe-0.02, and AgCe-0.03 exhibited an activation/deactivation process as their activity initially increased with time on stream, showing a maximum after which it began to decrease. In addition, only the deactivation process was observed over AgCe-0.04 and AgCe-0.05. The activation process was attributed to the reduction of Ce^{4+} by soot, leading to increased surface oxygen vacancies content and thereby active O_x^{n-} species generation. Conversely, the deactivation process was correlated to insufficient O_2^- delivery. The fact that, for AgCe-0, AgCe-0.01, AgCe-0.02, and AgCe-0.03, the deactivation process was initially overcome by the activation process, thanks to extra vacancies formation, confirmed that moderate initial vacancies content is essential for low-temperature good soot oxidation activity under GDI-like conditions.

Among the same lines, Wang et al. [46] studied several CeO_2-based catalysts where different contents of surface oxygen vacancies and active oxygen species (O_x^-) were modulated by means of high-temperature treatments, Ag doping, and O_3 activation. Again, according to soot-TPO measurements and to XPS/H_2-TPR/Raman analyses, a clear correlation between soot oxidation activity and O_x^- concentration was pointed out. As a matter of fact, the fresh CeO_2 (i.e., calcined at 500 °C) showed superior soot oxidation activity than CeO_2 aged at high-temperature (i.e., calcined at 800 °C) which was correlated to its higher O_x^- generation ability, resulting from proper surface oxygen vacancies amounts. In addition, the treatment of fresh CeO_2 in ozone increased the amounts of O_x^- species at the expense of excessive surface oxygen vacancies, thus improving soot oxidation activity. Similarly, the beneficial effect of silver loading was explained with the increased of the O_x^- concentration over CeO_2 via activation of both gas phase O_2 and ceria lattice oxygen. Interestingly, silver loading on the aged CeO_2 system (i.e., the least active

system) resulted in the most active catalyst. From XPS analyses, this was associated to the highest availability of ceria lattice oxygen, which was indicated as a potential source of O_x^- species with the assistance of Ag. Accordingly, as revealed by H_2-TPR and Raman results, the aged-Ag–CeO_2 catalyst exhibited the highest amounts of O_x^- species.

Additionally, Wu et al. [47] investigated Ag/CeO_2 catalysts focusing on the effect of both surface oxygen vacancies and bulk oxygen vacancies on soot oxidation performance. For this purpose, three types of CeO_2 catalysts with different combinations of surface and bulk oxygen vacancies were synthesized by precipitation methods at 30 °C, 50 °C, and 70 °C (i.e., named CeO_2-30, CeO_2-50, and CeO_2-70, respectively). They were then impregnated with Ag (5 wt.%). Under oxygen-rich conditions (20% O_2), the activity of the Ag/CeO_2 catalysts followed the order Ag/CeO_2-30 > Ag/CeO_2-50 > Ag/CeO_2-70, which was in line with the amounts of surface oxygen vacancies according to XPS results. Additionally, their activities in an oxygen-poor atmosphere (1% O_2) was Ag/CeO_2-30 ≈ Ag/CeO_2-50 > Ag/CeO_2-70, which in turn was correlated to the amounts of bulk oxygen vacancies. Of note, Ag/CeO_2-50 not only exhibited a similar activity to Ag/CeO_2-30, but also higher stability under repeated TPO oxidation cycles. Therefore, the moderate concentration of surface and bulk oxygen vacancies was indicated as essential for both the activity and stability of Ag/Ce-based systems under oxygen-poor conditions for use in GPF.

Kim et al. [48] investigated Ag-based catalysts focusing on the effect of support. For this purpose, they compared the soot oxidation activities of Ag/CeO_2 with that of samples prepared by impregnating the same amount of Ag (5 wt.%) on different types of TiO_2 (i.e., pure anatase, pure rutile, and P25, which contains both anatase and rutile phases). The activity of bare supports (i.e., without Ag) was also investigated. Air-TGA experiments under tight contact conditions showed the higher activity of CeO_2 than all TiO_2 samples, in line with its higher redox properties and oxygen storage capacity. Additionally, after the addition of silver, Ag/P25 and Ag/rutile catalysts showed higher activity than Ag/anatase and notably almost the same activities as Ag/CeO_2. The good performance of Ag/P25 and Ag/rutile was explained on the basis of XPS results, which showed that Ag/P25 and Ag/rutile included more oxidized silver species compared with Ag/anatase and Ag/CeO_2. Hence, soot oxidation activities were correlated with their higher oxidation properties at low temperature, as demonstrated by H_2-TPR results. As expected, when the same experiments were performed under loose contact conditions the combustion of soot was greatly decreased, particularly for TiO_2-based catalysts, which was attributed to the low contact between silver and soot under loose contact conditions. To improve the loose contact activity of the Ag/P25 catalyst, CeO_2 (3 wt.%) was impregnated on Ag/P25. The so obtained CeO_2–Ag/P25 catalyst showed higher loose contact activity than both Ag/P25 and Ag/CeO_2 (with T_{50} = 514 °C vs. 567 °C and 548 °C, respectively) pointing out a synergistic effect between the active oxygen supply ability of silver on P25 and the oxygen transfer ability of loaded CeO_2. The thermal stability of the catalyst via oxidation recycling experiments up to 800 °C and the oxidation activity under GPF conditions (1% O_2) were also verified in view of practical GDI applications.

As Ag/CeO_2 catalysts have been blamed for possible deactivation after aging at high temperatures [49] several strategies were proposed to improve catalysts stability. On this regard, Gao et al. [50] investigated Ag/CeO_2 catalysts doped with Nd (i.e., Ag/$Ce_xNd_{1-x}O_2$ with x = 1, 0.95, or 0.9) by analyzing the effect of Nd addition on both catalytic activity and stability. For this purpose, both TPO experiments (1%O_2) were performed over fresh (F) and aged (A) catalysts (i.e., treated at 700 °C in O_2 (1%)/H_2O (10%) for 48 h) under loose contact conditions. The catalytic activity was found to follow the order AgCe-F (T_m = °C 394 °C) > AgCe$Nd_{0.05}$-F (413 °C) > AgCe$Nd_{0.05}$-A (439 °C) > AgCe-A(448 °C) > AgCe$Nd_{0.1}$-F (455 °C) ≈ AgCe$Nd_{0.1}$-A (458 °C), thus suggesting that the introduction of Nd decreases the activity of Ag/CeO_2, but increases its thermal stability. Basing on XRD, XPS, and Raman analyses, the detrimental effect of Nd doping on soot oxidation activity that was observed for fresh catalysts was correlated to the increased formation

of ceria surface oxygen vacancies, and also to the reduced availability of bulk oxygen vacancies. Excessive surface oxygen vacancies were supposed responsible for less efficient activation of gas phase O_2, via formation of less active O^{2-} species instead of the highly active O_2^- ones. Conversely, regarding the aged catalysts, the positive effect of Nd doping was mainly ascribed to its inhibition effect on Ag growth and sintering, as evidenced by HRTEM, which improved the catalysts stability towards high temperatures. As a matter of fact, according to H_2-TPR results, the ability to generate active Ox^- species was retained for Nd-doped catalysts even after thermal aging, while it was significantly suppressed for the bare $AgCeO_2$. Accordingly, the addition of Nd into Ag/CeO_2 formulations was indicated as more practical for GDI applications, and particularly $Ag/Ce_{0.95}Nd_{0.05}O_2$ was suggested as a good balance between the catalyst activity and stability.

Of note, Gao et al. [51] focused on the thermal stability of Ag-based catalysts under gasoline oxidation conditions (i.e., 1% O_2). For this purpose, they compared fresh and spent Ag/Al_2O_3 catalysts, i.e., as prepared and aged in oxygen at 600 °C. The behavior of both fresh and spent Ag-catalysts with sulphated support was also addressed. The sulphated catalysts exhibited better activities than the others, and the spent catalysts behaved slightly better than the fresh ones. In situ TEM analyses revealed silver aggregation for Ag/Al_2O_3 during soot combustion. On the contrary, silver aggregation was mostly suppressed for sulphated Ag/Al_2O_3, where silver particles at the interface between soot and catalysts remained stationary during soot oxidation. In other words, the sulphation of alumina was suggested to anchor silver species (e.g., in the forms of Ag_2SO_4, according to XRD results) thus inhibiting silver aggregation and leading to higher soot oxidation activity. Redispersion of silver particles was also observed under increasing oxidative conditions, which explained the superior activities of the spent catalysts, particularly for the spent sulphated sample.

In order to prevent Ag sintering, and also its possible loss via Ag_2O vaporization, Wang et al. [52] developed confined catalysts with Ag protected by alumina (i.e., Al_2O_3-coated Ag catalysts denoted as $Ag@Al_2O_3$ catalysts). Catalytic soot combustion of both fresh and aged catalysts (i.e., calcined at 550 and 800 °C, respectively) was evaluated by TPO experiments in O_2 (1% *v/v* in N_2) under loose contact conditions. While the fresh catalysts led to a poor soot oxidation activity (T_{50} = 530 °C), the aged catalysts showed good catalytic performance (T_{50} = 460 °C). These results were explained in relation to the different morphologies and red-ox properties of both systems. According to TEM, XRD and BET analyses, the fresh catalyst showed large Ag particles (~28 nm) embedded inside micro porous and amorphous alumina, resulting in the low accessibility of Ag sites by soot and, thus, in a poor soot oxidation activity. Additionally, the aging treatment at 800 °C led to the conversion of the amorphous Al_2O_3 shell into mesoporous γ-Al_2O_3, and to the redispersion of Ag (~2.4 nm) both inside and on the external surface of alumina, resulting in an increased catalyst–soot contact and, thus, in a good soot oxidation capacity. In addition, H_2-TPR analyses performed over pre-oxidized samples showed the presence of higher amounts of Ag_xO species for the aged catalyst, indicating its high redox ability in line with its higher soot oxidation activity. Moreover, according to ICP results, almost no silver loss caused by high-temperature aging treatment was detected, which made the aged sample a good candidate for gasoline particulate filter catalysts applications.

A new generation of Ag-promoted $Fe_2O_3@CeO_2$ core-shell catalysts was further developed by Wang et al. [53]. In this case, a CeO_2 layer was grafted onto a Fe_2O_3 core and then silver (5 wt.%) was loaded on CeO_2 shell. In particular, iron oxides cores with different morphologies (i.e., cubes, rhombohedrons, and octadecahedrons denoted as Fe-C, Fe-R and Fe-O, respectively) were prepared in order to study the effect of different F_2O_3 crystal planes exposure on soot oxidation. The soot oxidation activity of $Ag/Fe_2O_3@CeO_2$ catalysts was investigated via TPO (Figure 6) and isothermal experiments (1%O_2) both under loose and tight contact conditions. For comparison purposes, tests were also performed over $Fe_2O_3@CeO_2$ catalysts (i.e., without Ag), over un-coated Fe_2O_3 (i.e., without CeO_2 shell), over Ag/Fe_2O_3 catalysts, and over CeO_2 (with and without Ag). The results

collected over bare Fe-oxides showed lower reactivity if compared with CeO_2. Notably, among them, the Fe-O sample (exposing mainly {113} planes) was superior to Fe-C and Fe-R samples (exposing either {012} or {014} planes) pointing out the crucial role of F_2O_3 crystal plane on soot oxidation. The high performance of Fe-O was in line with their high contents of O_x^- surface species, as indicated by Raman analyses, and it was explained on the basis of the electron-rich state of Fe atoms on Fe-O {113} planes. The promotion of CeO_2 coating on Fe_2O_3 was also observed; as a matter of fact, the Fe_2O_3@CeO_2 catalysts exhibited higher soot oxidation activity and stability than their corresponding Fe samples. In addition, they showed remarkably better activity than bare CeO_2. XPS results revealed the presence of surface Fe^{2+} only for Fe_2O_3@CeO_2 catalysts as a consequence of a very strong Fe_2O_3–CeO_2 interaction, leading to the oxygen transfer from Fe_2O_3 to CeO_2. This was confirmed by the low Ce^{3+} content observed over the Fe_2O_3–CeO_2 catalysts, indicating that oxygen vacancies of the CeO_2 shells were refilled readily by oxygen from the Fe_2O_3 cores. This oxygen delivery from Fe_2O_3 to CeO_2 was directly correlated to the fast generation of O_x^- surface species and, thus, to the improved soot oxidation activity of Fe_2O_3@CeO_2 core-shell catalysts.

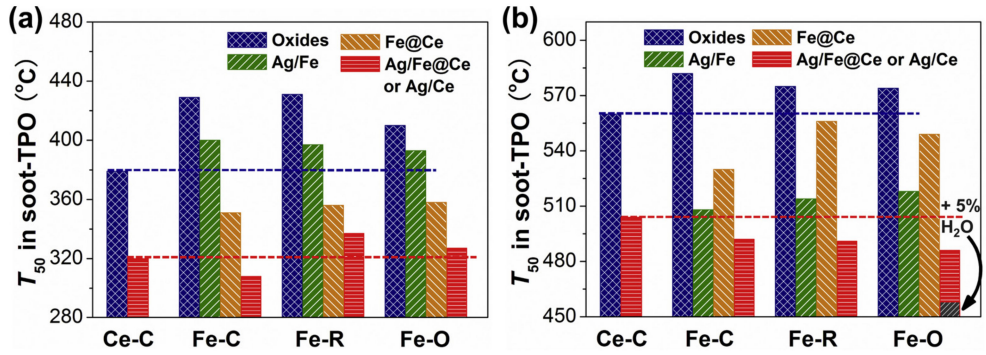

Figure 6. T_{50} during TPO under (**a**) "tight" contact and (**b**) "loose" contact. Reaction conditions: 1% O_2/N_2 (500 mL/min), heating rate = 5 °C/min, and catalyst/soot = 10/1. Reproduced with permission of reference [53].

A significant effect of silver on soot oxidation was observed, particularly for Ag/Fe_2O_3@CeO_2 catalysts. According to Raman and H_2-TPR results, this was ascribed to the ability of silver to increase the formation and regeneration of oxygen surface species by favoring the utilization of ceria bulk oxygen. In addition, the activation of gaseous O_2 on Ag nanoparticles leading to the formation of extra oxygen surface species (O_x^-) was also invoked.

Thanks to the above depicted $Fe_2O_3 \rightarrow CeO_2 \rightarrow Ag$ tandem delivery of oxygen, Ag/Fe_2O_3@CeO_2 materials emerged as promising catalysts for GPF, both in terms of soot oxidation activity (i.e., higher than Ag/CeO_2) and cost-efficiency (thanks to the low cost of Fe_2O_3).

Wang et al. [54] also investigated Ag/Co_3O_4@CeO_2 core-shell catalysts by replacing Fe_2O_3 with Co_3O_4. The soot oxidation activity was evaluated, both in O_2 (1%) and NO (500ppm) + O_2 (5%), in view of gasoline and diesel applications, respectively. In both cases, the comparison between Ag/Co_3O_4@CeO_2 and Ag/Fe_2O_3@CeO_2 catalysts revealed that the substitution of the Fe_2O_3 core by Co_3O_4 lead to catalysts with better soot oxidation activity. In particular, under both tight and loose contact conditions the T_{50} of Ag/Co_3O_4@CeO_2 were found ca. 30 °C lower that of Ag/Fe_2O_3@CeO_2 during O_2-TPO (i.e., ca. 280 °C and 460 °C vs. 310 °C and 490 °C, respectively). According to Raman and H_2-TPR characterization results, this was ascribed to the higher bulk oxygen exploitation for Co in comparison to Fe through a more efficient tandem oxygen delivery route (i.e., $Co_3O_4 \rightarrow CeO_2 \rightarrow Ag$), resulting in the formation of higher amounts of O_x^- species. On the one hand, these active oxygen species were suggested to favor the direct combustion of soot via O_2-route and,

on the other, to promote the NO→NO_2 conversion, and thus the low temperature soot oxidation via NO_2-route. The reactivity of $Ag/Co_3O_4@CeO_2$ was further evaluated under more realistic conditions (i.e., in the presence of H_2O (5%) and even, after hydrothermal ageing, in 10% H_2O/air at 800 °C). The comparison with Pt/Al_2O_3, i.e., a well-known catalyst for NO and soot oxidation, was also provided. Thanks to its high activity and good hydrothermal stability (Figure 7), $Ag/Co_3O_4@CeO_2$ proved to be a promising option for application in both gasoline and diesel filters.

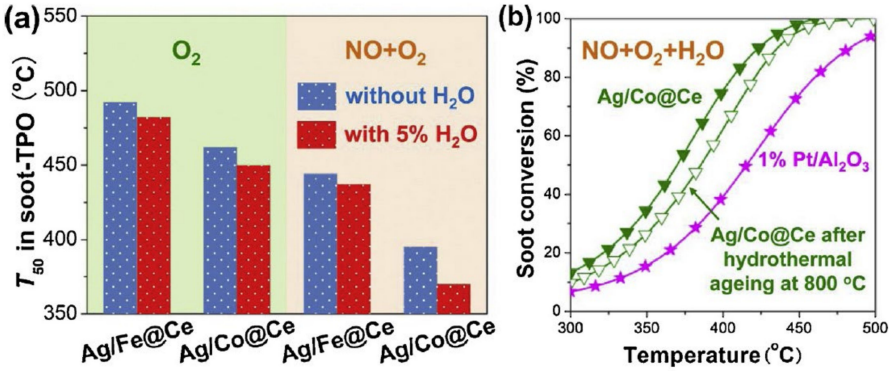

Figure 7. Soot oxidation behavior of the catalysts under (**a**) O_2(1%) or 500(ppm NO)/O_2(5%), with or without 5% H_2O, and (**b**) 500(ppm NO)/O_2(5%)/H_2O(5%): effect of hydrothermal aging and comparison with Pt/Al_2O_3. Reaction conditions: catalyst/soot = 10/1 ("loose" contact mode), TPO heating rate = 5 °C/min. Reproduced with permission of reference [54].

Notably, very recently, Liang et al. proposed the alternative use of Ag-doped yttria-stabilized zirconia (YSZ) catalysts, instead of Ag/ceria-based materials, in light of the YSZ high thermal/chemical stability [55]. In particular, they investigated Ag/YSZ catalysts with macroporous fiber-like morphology, which showed remarkable activity even after aging (i.e., at 800 °C for 10 h) during TPO in O_2(1%)/H_2O(5%) under loose contact conditions (i.e., T_{50} = 372 °C). On the one hand, the macroporous, fiber-like morphology was shown as essential to obtain good catalyst–soot contact. On the other hand, according to TEM, XPS, H_2-TPR, and Raman analyses, the redispersion of silver after aging was indicated as responsible for high reducibility and oxygen species (i.e., O^-) availability leading to superior soot oxidation activity.

Cu-doped Ceria/zirconia catalysts have been also considered for gasoline application. García-García and co-workers [56] reported preliminary results on a Cu(2%)/ceria–zirconia catalyst that was investigated for soot oxidation under He atmosphere (i.e., without oxygen) in order to explore its application under normal GDI exhaust conditions. The corresponding Cu-free catalyst was also investigated for comparison purposes. TGA experiments on soot/catalyst mixtures under loose contact conditions were performed, and TGA, coupled with Mass Spectrometer analyses, were additionally performed on the fresh catalysts (i.e., without soot) in order to analyze the O_2 release under inert conditions. The introduction of Cu allowed the improvement of soot oxidation activity that was in line with the TG–MS results, which showed higher O_2 release (i.e., the source for O_2 catalyzed soot combustion), if compared with bare CZ. Accordingly, these results suggested copper/ceria–zirconia formulations as potential candidates for soot oxidation under GDI conditions.

Finally, Ashikaga et al. [57] systematically investigated the effect of loading transition metals onto CeO_2 focusing on the role of metal–support interactions in catalytic activity. For this purpose, M/CeO_2 catalysts (M = Mn, Fe, Co, Ni, Cu, Rh, Pd, and Ag) with 5 wt% metal loading were prepared and used for soot combustion under low oxygen concentration conditions (i.e., 0.5% O_2). The soot combustion activities increased in the following order: pure CeO_2 < Fe < Mn < Ag < Ni < Pd < Co < Cu and Rh (Figure 8). In particular, Cu/CeO_2 and Rh/CeO_2 displayed the highest soot combustion activity

with values of T_{10} ca.70 °C, lower than that for pure CeO_2 (i.e., ca. 265 °C vs. 335 °C, under tight conditions).

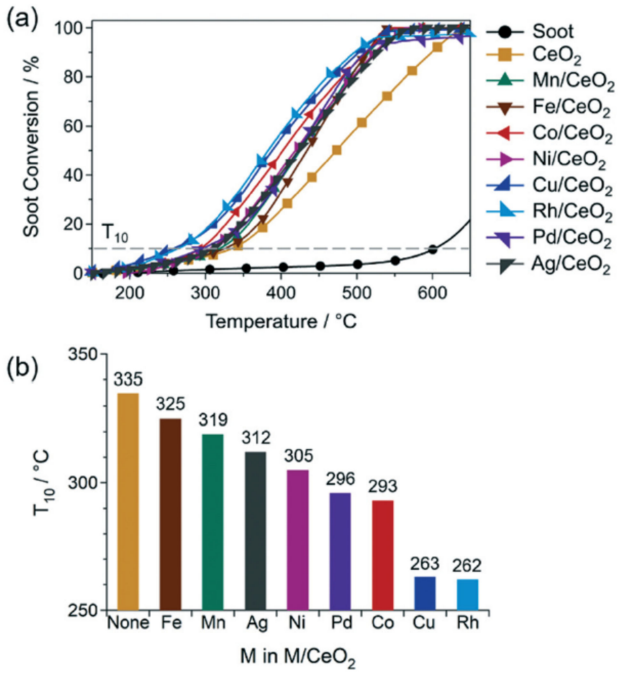

Figure 8. (**a**) Soot conversion versus temperature. (**b**) T_{10} in the presence of M/CeO_2 catalysts under a flow of 0.5% O_2. Reproduced with permission of reference [57].

For comparison purposes, the catalytic activity of the analogous M/SiO_2 catalysts was also analyzed, where chemically inert SiO_2 was used as the support instead of CeO_2. The activity of M/SiO_2 samples was remarkably lower than the corresponding M/CeO_2 samples. In fact, the T_{10} values for most M/SiO_2 catalysts were 500 °C or higher. This exhibited the specific role of metal–CeO_2 interaction in soot combustion. This was confirmed by comparing the soot oxidation activity of Cu/CeO_2 with that of a CuO + CeO_2 physical mixture, i.e., a system with a low Cu–CeO_2 interface. Notably, the T_{10} values for CuO + CeO_2 were similar to pure CeO_2, and higher than Cu/CeO_2 (i.e., 348 °C vs. 263 °C) thus indicating that the high soot combustion activity for Cu/CeO_2 was not related to the presence of the supported CuO_x species itself, but particularly to the close contact between Cu and CeO_2. According to H_2-TPR results, the close interaction between Cu and CeO_2 was indicated as responsible for the higher reducibility of Cu/CeO_2 than CuO + CeO_2 physical mixture. The authors further examined the reducibility and the oxygen release properties of all the M/CeO_2 samples in more detail, utilizing H_2-TPR and TGA-oxygen release measurements, respectively. They found a linear correlation between the oxygen release rate and the catalytic soot combustion activity (i.e., T_{10}). In turn, this was correlated with the strength of the interaction or chemical bond between the metal and support. In particular a volcano-shaped correlation between the oxygen release rate and the energy of the metal–oxygen (M–O) bond of the supported metal was found, with Cu and Rh at the top. Thus, the high soot combustion activity of CeO_2-supported Cu and Rh catalysts was attributed to their appropriate metal–CeO_2 interfaces, from which lattice oxygen can be easily released due to their moderate M–O bond energies. Additionally, the low activity of M/CeO_2 systems with higher M–O bond energies (e.g., Fe, Mn, Ni, and Co) was correlated to the formation of relatively strong M–O–Ce bonds, resulting in weak promotion of oxygen release of CeO_2. Conversely, the low activity of M/CeO_2 systems with lower M–O bond energies (e.g., Pd and Ag) was explained with the formation of an inadequate metal–CeO_2 interface, due to the weakness of the metal interaction with CeO_2. The authors definitively identified the selection of supported metal species with

moderate M–O bond energies as essential to optimize the oxygen release properties of CeO_2 via metal–support interactions and, thus, to increase the soot combustion activity of CeO_2-based catalysts under low oxygen concentration conditions.

3. Perovskite-Type Catalysts for Gasoline Soot Oxidation

Among the Pt-free catalysts suggested for O_2–soot oxidation, mixed oxides with perovskite structure (general formula ABO_3) were widely investigated and emerged as effective catalysts for diesel applications (e.g., see the reviews [30,58,59]), thanks to their high oxidation activity and thermo-stability. The catalytic activity depends on the nature of A and B cations, which can be suitably selected and/or partially substituted (general formula $A_{1-x}A'_xB_{1-x}B'_xO_3$) to favor catalytic properties essential for soot combustion, i.e., mobility of the catalysts' oxygen species, redox properties, and thermo-stability. More recently, in light of their versatility, perovskites were also proposed for gasoline applications.

Vernoux and co-workers studied $La_{0.6}Sr_{0.4}BO_3$-type perovskites (with B = Fe, Mn, or Ti) for soot combustion reaction under low amounts of oxygen content [60]. First of all, the soot combustion efficiency was investigated in the presence of 1% O_2 (v/v) by TPO experiments under tight conditions. The results showed a clear correlation between catalytic performances and perovskite redox properties. Among the investigated samples, the Ti-based system was the least efficient. As a matter of fact, the soot ignition temperature was close to 530 °C (i.e., the same of un-catalyzed soot) and T_{50} was seen near 675 °C. Additionally, CO_2 selectivity was not complete (i.e., 70%). Instead, Fe- and Mn-based systems gave interesting performances in soot oxidation, showing ignition temperatures of ca. 430 °C (i.e., more 100 °C below that of the un-catalyzed soot) and T_{50} near 535 °C (i.e., about 140 °C below that of Ti-based system). Additionally, the CO_2 selectivity was increased above 99%. Fe and Mn-perovskites were further investigated under lower oxygen partial pressure (i.e., 0.2% O_2), and without any O_2. TPO results with 0.2% O_2 were very similar to those performed with 1% of O_2, i.e., leading to similar ignition temperatures, but after ignition the soot combustion preceded more slowly, being limited by the low oxygen partial pressure. In addition, TPO results collected under inert condition (0% O_2 in He) showed very low soot conversion (i.e., 8.5 and 9.5% for Fe- and Mn-perovskites, respectively) as it was only ascribed to the available oxygen surface species. In both cases, below 500 °C, the Fe-perovskite showed the best performances, conversely above 500 °C the Mn-perovskite was significantly better. The authors attributed the poor reactivity of Ti-perovskite to its negligible oxygen release capacity and reducibility, according to O_2-TPD and H_2-TPR experiments, respectively. Instead, they ascribed the good performances of the Fe-perovskite, particularly below 500 °C, to the presence of efficient surface oxygen vacancies, which favor oxygen transfer and, as a result, soot combustion. On the other side, above 500 °C for the Mn-perovskite, they suggested the key role of Mn^{4+} cations in transfer bulk oxygen to the catalyst–soot contact points, particularly at low oxygen partial pressures, i.e., typical condition of GDI exhaust.

The impact of manganites and ferrites substitution by Ag cations was further investigated. Hernández et al. [61] studied LaSrxAgMn and LaSrxAgFe perovskites by varying the silver content (x) from 5 to 25% molar ratio with respect to the total A-site ions (La + Sr + Ag). Their catalytic performances were investigated for the soot oxidation with TPO at low O_2 partial pressure (1%), under tight conditions. The results showed that the addition of silver improves soot oxidation in all cases. However, for ferrites, the promotion was rather limited, and mostly insensitive to silver loading. Instead, the substitution by Ag was found to significantly enhance the activity of manganites, that increased upon increasing the Ag content. In particular, for the LaSr25AgMn catalyst, the onset temperature for soot oxidation was near 370 °C, i.e., about 60 °C below that of the undoped LaSrMn. This also led to a decrease in the T_{50} near 450 °C (i.e., about 90 °C below LaSrMn). The authors showed a close relationship between the location, size, and chemical nature of Ag, and the catalytic performances of the different perovskites. Based on TEM and XRD analyses, they attributed the lower activity of LaSrxAgFe to the incorporation of Ag^+ cations in the

perovskite structure, and to the presence of large Ag particles on the surface, including agglomerates. Particularly for high Ag contents, these agglomerates are expected to cover the perovskites surface, including the oxygen vacancies, thus decreasing their oxygen transfer capacity. On the contrary, for manganites, Ag was mainly present as surface Ag/AgO_x nanoparticles, or as a surface $Ag_{1.8}Mn_8O_{16}$ additional hollandite-type phase. According to O_2-TPD and H_2-TPR results, both of them were indicated to improve the reducibility and the oxygen storage capacity of manganites, thus boosting their soot oxidation capacity. In addition, the authors explained the higher catalytic performance of LaSrxAgMn on the basis of their macroporous morphology, which is expected to favor a more intimate catalyst–soot contact and, as a result, higher catalyst–soot interactions. All these findings highlighted Ag modified manganites as promising materials for catalyzed gasoline particulate filters.

The effect of partial copper incorporation into iron-based perovskites have been also investigated. For this purpose, Illán-Gómez and co-workers [62] worked on a series of $BaFe_{1-x}Cu_xO_3$ perovskites (x = 0, 0.1, 0.3, and 0.4) which were investigated for soot oxidation under inert conditions, i.e., under very demanding conditions of regular stoichiometric GDI operation. For this purpose, Temperature Programmed Reactions were performed only in He under loose contact conditions. This revealed that all catalysts are active for soot combustion in the absence of oxygen at temperatures higher than ca. 550 °C, and that the soot oxidation activity increases upon increasing Cu content. In particular, the soot conversion increased with the copper content, from 29% without Cu, up to 94% for the sample with the highest Cu content (i.e., $BaFe_{0.6}Cu_{0.4}O_3$). According to O_2-TPD experiments, the highest soot conversion shown by the highest copper content catalyst was ascribed to the largest evolution of β-oxygen, i.e., lattice oxygen, which is evolved at the high temperatures (i.e., coming from the reduction of Fe), where soot combustion occurs. In addition, for materials with the highest copper loading, XPS and XRD results revealed the presence of high amounts of surface copper species (e.g., BaO_x–CuO_x oxide), which were related to the increased soot removal.

Torregrosa-Rivero et al. [63] deepened the soot oxidation performance of $BaFe_{1-x}Cu_xO_3$ catalysts (x = 0, 0.1, 0.3, and 0.4) in the presence of oxygen. For this purpose, TPO with 1% O_2 in He were performed, in order to work under "fuel cuts" GDI exhaust conditions. All the catalysts were found to markedly increase the selectivity of soot combustion to CO_2 if compared to bare soot. On the other hand, a limited effect on soot ignition, mostly limited to $BaFeO_3$ and $BaFe_{0.9}Cu_{0.1}O_3$ perovskites (i.e., the catalyst without Cu and that with the lowest Cu content, respectively), was observed. This was mainly correlated to the overall amounts of oxygen released during O_2-TPD, which was found to decrease upon increasing copper content. The comparison of these results with those previously obtained under inert conditions [62] pointed out that copper incorporation into the $BaFeO_3$ perovskite structure positively impacts the catalytic soot combustion, particularly in the absence of oxygen.

4. Conclusions

Ceria-based and perovskites-type materials have been extensively investigated as suitable catalysts for diesel particulate filters applications whereas their possible use in gasoline filters is still at the initial stage. However, as it clearly appears from the increasing recent academic publications, both of them emerge as powerful candidates for soot oxidation under very demanding conditions of gasoline exhaust (i.e., under oxygen-poor environments), in light of their unique ability to promote the formation of active surface oxygen species.

The trend is moving towards multicomponent catalysts.

As for ceria-based formulations, (i) doping with foreign cations (e.g., Zr, Pr) and (ii) loading of metals (e.g., Ag, Cu) are being exploited, not only to improve the thermal stability of pure ceria (i.e., by preserving efficient soot–catalyst contact during soot combustion), but also to promote its oxygen storage/redox properties and, consequently, its catalytic properties. Regarding the latter, the formation of proper amounts of oxygen

vacancies at the interface between ceria and soot seems to be essential to obtain active surface oxygen species for soot oxidation. In particular, among the promotion methods, the potential of Ag doping has been mostly explored in view of its ability to promote the formation of active surface oxygen species via activation of both gaseous O_2 and ceria lattice oxygen. However, as Ag-catalysts can be affected by thermal deactivation it remains a challenge to find efficient and stable materials under soot oxidation conditions. In this context, the introduction of further dopants (e.g., Nd) to Ag/ceria catalysts, or the substitution of ceria with YSZ, have been indicated to increase the thermal stability for applications in GPFs. Additionally, core shell-like materials (e.g., $Ag/M_xO_y@CeO_2$ with M = Fe or Co) have been proposed, resulting in both high soot combustion activity (i.e., via a tandem oxygen delivery route ($M_xO_y \rightarrow CeO_2 \rightarrow Ag$) leading to an efficient transfer of bulk oxygen to soot), and high hydrothermal stability.

As for perovskites, La/Sr-based manganites and ferrites, even doped with Ag, and Cu-doped $BaFeO_3$, have been proven to oxidize soot at low oxygen contents, thanks to their redox properties and oxygen surface vacancies, by transporting bulk oxygen at the catalyst–soot interface.

An overall conclusion emerging from this survey is that, owing to their specific properties, particularly involving the efficient generation and exploitation of reactive oxygen surface species, the above reviewed ceria- and perovskite-based materials represent a good starting point for the development of catalysts for GDI soot oxidation with improved activity, selectivity, and stability, but also cost efficiency, as they aim at minimizing the use of noble metals.

Funding: This research received no external funding.

Acknowledgments: The author thanks Luca Lietti for useful discussion and suggestions.

Conflicts of Interest: The author declares no conflict of interest.

References

1. Joshi, A. Review of Vehicle Engine Efficiency and Emissions. *SAE Int. J. Adv. Curr. Pract Mobil.* **2020**, *2*, 2479–2507. [CrossRef]
2. Joshi, A.; Johnson, T.V. Gasoline Particulate Filters—A Review. *Emiss. Control. Sci. Technol.* **2018**, *4*, 219–239. [CrossRef]
3. Giechaskiel, B.; Joshi, A.; Ntziachristos, L.; Dilara, P. European Regulatory Framework and Particulate Matter Emissions of Gasoline Light-Duty Vehicles: A Review. *Catalysts* **2019**, *9*, 586. [CrossRef]
4. Neyestani, S.E.; Walters, S.; Pfister, G.; Kooperman, G.J.; Saleh, R.; Neyestani, S.E.; Walters, S.; Pfister, G.; Kooperman, G.J.; Saleh, R. Direct Radiative Effect and Public Health Implications of Aerosol Emissions Associated with Shifting to Gasoline Direct Injection (GDI) Technologies in Light-Duty Vehicles in the United States. *Environ. Sci. Technol.* **2019**, *54*, 687–696. [CrossRef] [PubMed]
5. Awad, O.; Ma, X.; Kamil, M.; Majeed, A.; Zhang, Z.; Shuai, S. Particulate emissions from gasoline direct injection engines: A review of how current emission regulations are being met by automobile manufacturers. *Sci. Total Environ.* **2020**, *718*, 137302. [CrossRef] [PubMed]
6. Luo, Y.; Zhu, L.; Fang, J.; Zhuang, Z.; Guan, C.; Xia, C.; Xie, X.; Huang, Z. Size distribution, chemical composition and oxidation reactivity of particulate matter from gasoline direct injection (GDI) engine fueled with ethanol-gasoline fuel. *Appl. Therm. Eng.* **2015**, *89*, 647–655. [CrossRef]
7. Qian, Y.; Li, Z.; Yu, L.; Wang, X.; Lu, X. Review of the state-of-the-art of particulate matter emissions from modern gasoline fueled engines. *Appl. Energy* **2019**, *238*, 1269–1298. [CrossRef]
8. Whitaker, P.; Kapus, P.; Ogris, M.; Hollerer, P. Measures to Reduce Particulate Emissions from Gasoline DI engines. *SAE Int. J. Engines* **2011**, *4*, 1498–1512. [CrossRef]
9. Guan, B.; Zhan, R.; Lin, H.; Huang, Z. Review of the state-of-the-art of exhaust particulate filter technology in internal combustion engines. *J. Environ. Manag.* **2015**, *154*, 225–258. [CrossRef]
10. Raza, M.; Chen, L.; Leach, F.; Ding, S. A Review of Particulate Number (PN) Emissions from Gasoline Direct Injection (GDI) Engines and Their Control Techniques. *Energies* **2018**, *11*, 1417. [CrossRef]
11. Piock, W.; Hoffmann, G.; Berndorfer, A.; Salemi, P.; Fusshoeller, B. Strategies Towards Meeting Future Particulate Matter Emission Requirements in Homogeneous Gasoline Direct Injection Engines. *SAE Int. J. Engines* **2011**, *4*, 1455–1468. [CrossRef]
12. Bromberg, L.; Cohn, D. Optimized PFI+DI Operation For Minimizing DI Gasoline Engine Particulates. *SAE Tech. Pap.* **2018**. [CrossRef]
13. Karavalakis, G.; Durbin, T.D.; Yang, J.; Ventura, L.; Xu, K. Fuel Effects on PM Emissions from Different Vehicle/Engine Configurations: A Literature Review. *SAE Tech. Pap.* **2018**. [CrossRef]

14. Twigg, M.V. Catalytic control of emissions from cars. *Catal. Today* **2011**, *163*, 33–41. [CrossRef]
15. Saito, C.; Nakatani, T.; Miyairi, Y.; Yuuki, K.; Makino, M.; Kurachi, H.; Heuss, W.; Kuki, T.; Furuta, Y.; Kattouah, P.; et al. New Particulate Filter Concept to Reduce Particle Number Emissions. *SAE Tech. Pap.* **2011**. [CrossRef]
16. Matarrese, R.; Castoldi, L.; Lietti, L. Oxidation of model soot by NO_2 and O_2 in the presence of water vapor. *Chem. Eng. Sci.* **2017**, *173*, 560–569. [CrossRef]
17. Hazlett, M.J.; Epling, W.S. Heterogeneous catalyst design: Zoned and layered catalysts in diesel vehicle aftertreatment monolith reactors. *Can. J. Chem. Eng.* **2018**, *97*, 188–206. [CrossRef]
18. Lanzerath, P.; Wunsch, R.; Schön, C. The first series-production particulate filter for Mercedes-Benz gasoline engines. In *17 Internationales Stuttgarter Symposium*; Bargende, M., Reuss, H.C., Wiedemann, J., Eds.; Springer: Vieweg, Wiesbaden, 2017; pp. 851–865. [CrossRef]
19. Joshi, A. Review of Vehicle Engine Efficiency and Emissions. *SAE Int. J. Adv. Curr. Pract. Mobil.* **2019**, *1*, 734–761. [CrossRef]
20. Johnson, T.; Joshi, A. Review of Vehicle Engine Efficiency and Emissions. *SAE Int. J. Engines* **2018**, *11*, 1307–1330. [CrossRef]
21. Joshi, A. Progress and Outlook on Gasoline Vehicle Aftertreatment Systems. *Johns. Matthey Technol. Rev.* **2017**, *61*, 311–325. [CrossRef]
22. Zhan, R.; Eakle, S.T.; Weber, P.A. Simultaneous Reduction of PM, HC, CO and NO_x Emissions from a GDI Engine. *SAE Tech. Pap.* **2010**. [CrossRef]
23. Richter, J.M.; Klingmann, R.; Spiess, S.; Wong, K.-F.; Richter, J.M.; Klingmann, R.; Spiess, S.; Wong, K.-F. Application of Catalyzed Gasoline Particulate Filters to GDI Vehicles. *SAE Int. J. Engines* **2012**, *5*, 1361–1370. [CrossRef]
24. Liu, X.; Chanko, T.; Lambert, C.; Maricq, M. Gasoline Particulate Filter Efficiency and Backpressure at Very Low Mileage. *SAE Tech. Pap.* **2018**. [CrossRef]
25. Johnson, T. Vehicular Emissions in Review. *SAE Int. J. Engines* **2014**, *7*, 1207–1227. [CrossRef]
26. Johnson, T.; Joshi, A. Review of Vehicle Engine Efficiency and Emissions. *SAE Tech. Pap.* **2017**. [CrossRef]
27. Available online: https://dieselnet.com/tech/gasoline_particulate_filters.php (accessed on 21 June 2021).
28. Neeft, J.P.A.; Makkee, M.; Moulijn, J.A. Metal oxides as catalysts for the oxidation of soot. *Chem. Eng. J. Biochem. Eng. J.* **1996**, *64*, 295–302. [CrossRef]
29. Van Setten, B.A.A.L.; Makkee, M.; Moulijn, J.A. Science and technology of catalytic diesel particulate filters. *Catal. Rev.* **2001**, *43*, 489–564. [CrossRef]
30. Hernández-Giménez, A.M.; Castelló, D.L.; Bueno-López, A. Diesel soot combustion catalysts: Review of active phases. *Chem. Pap.* **2014**, *68*, 1154–1168. [CrossRef]
31. Fino, D.; Bensaid, S.; Piumetti, M.; Russo, N. A review on the catalytic combustion of soot in Diesel particulate filters for automotive applications: From powder catalysts to structured reactors. *Appl. Catal. A Gen.* **2016**, *509*, 75–96. [CrossRef]
32. Bueno-López, A. Diesel soot combustion ceria catalysts. *Appl. Catal. B Environ.* **2014**, *146*, 1–11. [CrossRef]
33. Trovarelli, A.; Llorca, J. Ceria Catalysts at Nanoscale: How Do Crystal Shapes Shape Catalysis? *ACS Catal.* **2017**, *7*, 4716–4735. [CrossRef]
34. Wang, R.; Lan, L.; Gong, M.-C.; Chen, Y.-Q. Catalytic Combustion of Gasoline Particulate Soot over CeO_2-ZrO_2 Catalysts. *Acta Phys.-Chim. Sin.* **2016**, *32*, 1747–1757. [CrossRef]
35. Sun Park, C.; Lee, M.W.; Lee, J.H.; Jeong, E.J.; Lee, S.H.; Choung, J.W.; Kim, C.H.; Ham, H.C.; Lee, K.-Y. Promoting effect of H_2O over macroporous Ce-Zr catalysts in soot oxidation. *Mol. Catal.* **2019**, *474*, 110416. [CrossRef]
36. Liu, P.; Liang, X.; Dang, Y.; He, J.; Shirazi-Amin, A.; Achola, L.A.; Dissanayake, S.; Chen, H.; Fu, M.; Ye, D.; et al. Effects of Zr substitution on soot combustion over cubic fluorite-structured nanoceria: Soot-ceria contact and interfacial oxygen evolution. *J. Environ. Sci.* **2021**, *101*, 293–303. [CrossRef] [PubMed]
37. Liu, S.; Wu, X.D.; Tang, J.; Cui, P.Y.; Jiang, X.Q.; Chang, C.G.; Liu, W.; Gao, Y.X.; Li, M.; Weng, D. An exploration of soot oxidation over CeO_2-ZrO_2 nanocubes: Do more surface oxygen vacancies benefit the reaction? *Catal. Today* **2017**, *281*, 454–459. [CrossRef]
38. Aneggi, E.; Trovarelli, A. Potential of Ceria-Zirconia-Based Materials in Carbon Soot Oxidation for Gasoline Particulate Filters. *Catalysts* **2020**, *10*, 768. [CrossRef]
39. Martínez-Munuera, J.C.; Zoccoli, M.; Giménez-Mañogil, J.; Garcia-Garcia, A. Lattice oxygen activity in ceria-praseodymia mixed oxides for soot oxidation in catalysed Gasoline Particle Filters. *Appl. Catal. B Environ.* **2019**, *245*, 706–720. [CrossRef]
40. Sartoretti, E.; Martini, F.; Piumetti, M.; Bensaid, S.; Russo, N.; Fino, D. Nanostructured Equimolar Ceria-Praseodymia for Total Oxidations in Low-O_2 Conditions. *Catalysts* **2020**, *10*, 165. [CrossRef]
41. Yao, P.; He, J.; Jiang, X.; Jiao, Y.; Wang, J.; Chen, Y. Factors determining gasoline soot abatement over CeO_2–ZrO_2-MnO_x catalysts under low oxygen concentration condition. *J. Energy Inst.* **2020**, *93*, 774–783. [CrossRef]
42. Yang, W.N.; Wang, S.M.; Li, K.Z.; Liu, S.; Gan, L.N.; Peng, Y.; Li, J.H. Highly selective α-Mn_2O_3 catalyst for cGPF soot oxidation: Surface activated oxygen enhancement via selective dissolution. *Chem. Eng. J.* **2019**, *364*, 448–451. [CrossRef]
43. Xiong, L.; Yao, P.; Liu, S.; Li, S.; Deng, J.; Jiao, Y.; Chen, Y.; Wang, J. Soot oxidation over CeO_2-ZrO_2 based catalysts: The influence of external surface and low-temperature reducibility. *Mol. Catal.* **2019**, *467*, 16–23. [CrossRef]
44. Liu, S.; Wu, X.D.; Liu, W.; Chen, W.M.; Ran, R.; Li, M.; Weng, D. Soot oxidation over CeO_2 and Ag/CeO_2: Factors determining the catalyst activity and stability during reaction. *J. Catal.* **2016**, *337*, 188–198. [CrossRef]
45. Wang, H.L.; Liu, S.; Zhao, Z.; Zou, X.; Liu, M.H.; Liu, W.; Wu, X.D.; Weng, D. Activation and deactivation of Ag/CeO_2 during soot oxidation: Influences of interfacial ceria reduction. *Catal. Sci. Technol.* **2017**, *7*, 2129–2139. [CrossRef]

46. Wang, H.; Luo, S.; Zhang, M.; Liu, W.; Wu, X.; Liu, S. Roles of oxygen vacancy and O_x- in oxidation reactions over CeO_2 and Ag/CeO_2 nanorod model catalysts. *J. Catal.* **2018**, *368*, 365–378. [CrossRef]
47. Wu, S.J.; Yang, Y.; Lu, C.X.; Ma, Y.Y.; Yuan, S.X.; Qian, G.R. Soot Oxidation over CeO_2 or Ag/CeO_2: Influences of Bulk Oxygen Vacancies and Surface Oxygen Vacancies on Activity and Stability of the Catalyst. *Eur. J. Inorg. Chem.* **2018**, *2018*, 2944–2951. [CrossRef]
48. Kim, M.J.; Han, G.-H.; Lee, S.H.; Jung, H.W.; Choung, J.W.; Kim, C.H.; Lee, K.-Y. CeO_2 promoted Ag/TiO_2 catalyst for soot oxidation with improved active oxygen generation and delivery abilities. *J. Hazard. Mater.* **2020**, *384*, 121341. [CrossRef] [PubMed]
49. Aneggi, E.; Llorca, J.; de Leitenburg, C.; Dolcetti, G.; Trovarelli, A. Soot combustion over silver-supported catalysts. *Appl. Catal. B Environ.* **2009**, *91*, 489–498. [CrossRef]
50. Gao, Y.X.; Duan, A.Q.; Liu, S.; Wu, X.D.; Liu, W.; Li, M.; Chen, S.G.; Wang, X.; Weng, D. Study of $Ag/Ce_xNd_{1-x}O_2$ nanocubes as soot oxidation catalysts for gasoline particulate filters: Balancing catalyst activity and stability by Nd doping. *Appl. Catal. B Environ.* **2017**, *203*, 116–126. [CrossRef]
51. Gao, Y.; Wu, X.; Liu, S.; Ogura, M.; Liu, M.; Weng, D. Aggregation and redispersion of silver species on alumina and sulphated alumina supports for soot oxidation. *Catal. Sci. Technol.* **2017**, *7*, 3524–3530. [CrossRef]
52. Wang, H.L.; Luo, S.T.; Li, X.H.; Liu, W.; Wu, X.D.; Weng, D.; Liu, S. Thermally stable Ag/Al_2O_3 confined catalysts with high diffusion-induced oxidation activity. *Catal. Today* **2019**, *332*, 189–194. [CrossRef]
53. Wang, H.; Jin, B.; Wang, H.; Ma, N.; Liu, W.; Weng, D.; Wu, X.; Liu, S.; Wang, H.; Jin, B.; et al. Study of Ag promoted $Fe_2O_3@CeO_2$ as superior soot oxidation catalysts: The role of Fe_2O_3 crystal plane and tandem oxygen delivery. *Appl. Catal. B Environ.* **2018**, *237*, 251–262. [CrossRef]
54. Wang, X.; Jin, B.; Feng, R.; Liu, W.; Weng, D.; Wu, X.; Liu, S. A robust core-shell silver soot oxidation catalyst driven by Co_3O_4: Effect of tandem oxygen delivery and Co_3O_4-CeO_2 synergy. *Appl. Catal. B Environ.* **2019**, *250*, 132–142. [CrossRef]
55. Liang, H.; Jin, B.; Li, M.; Yuan, X.; Wan, J.; Liu, W.; Wu, X.; Liu, S. Highly reactive and thermally stable Ag/YSZ catalysts with macroporous fiber-like morphology for soot combustion. *Appl. Catal. B Environ.* **2021**, *294*, 120271. [CrossRef]
56. Giménez-Mañogil, J.; Quiles-Díaz, S.; Guillén-Hurtado, N.; García-García, A. Catalyzed Particulate Filter Regeneration by Platinum Versus Noble Metal-Free Catalysts: From Principles to Real Application. *Top. Catal.* **2016**, *60*, 2–12. [CrossRef]
57. Ashikaga, R.; Murata, K.; Ito, T.; Yamamoto, Y.; Arai, S.; Satsuma, A. Tuning the oxygen release properties of CeO_2-based catalysts by metal–support interactions for improved gasoline soot combustion. *Catal. Sci. Technol.* **2020**, *10*, 7177–7185. [CrossRef]
58. Mishra, A.; Prasad, R. Preparation and Application of Perovskite Catalysts for Diesel Soot Emissions Control: An Overview. *Catal. Rev.* **2014**, *56*, 57–81. [CrossRef]
59. Royer, S.; Duprez, D.; Can, F.; Courtois, X.; Batiot-Dupeyrat, C.; Laassiri, S.; Alamdari, H. Perovskites as Substitutes of Noble Metals for Heterogeneous Catalysis: Dream or Reality. *Chem. Rev.* **2014**, *114*, 10292–10368. [CrossRef]
60. Hernández, W.Y.; Tsampas, M.Y.; Zhao, C.N.; Boreave, A.; Bosselet, F.; Vernoux, P. La/Sr-based perovskites as soot oxidation catalysts for Gasoline Particulate Filters. *Catal. Today* **2015**, *258*, 525–534. [CrossRef]
61. Hernández, W.Y.; Lopez-Gonzalez, D.; Ntais, S.; Zhao, C.; Boréave, A.; Vernoux, P. Silver-modified manganite and ferrite perovskites for catalyzed gasoline particulate filters. *Appl. Catal. B Environ.* **2018**, *226*, 202–212. [CrossRef]
62. Moreno-Marcos, C.; Torregrosa-Rivero, V.; Albaladejo-Fuentes, V.; Sánchez-Adsuar, M.S.; Illán-Gómez, M.J. $BaFe_{1-x}Cu_xO_3$ Perovskites as Soot Oxidation Catalysts for Gasoline Particulate Filters (GPF): A Preliminary Study. *Top. Catal.* **2018**, *62*, 413–418. [CrossRef]
63. Torregrosa-Rivero, V.; Moreno-Marcos, C.; Albaladejo-Fuentes, V.; Sánchez-Adsuar, M.-S.; Illán-Gómez, M.-J.; Rivero, T.; Marcos, M.; Fuentes, A.; Adsuar, S.; Gómez, I. $BaFe_{1-x}Cu_xO_3$ Perovskites as Active Phase for Diesel (DPF) and Gasoline Particle Filters (GPF). *Nanomaterials* **2019**, *9*, 1551. [CrossRef] [PubMed]